IEEE Access
Multidisciplinary | Rapid Review | Open Access Journal

Received April 15, 2019, accepted July 8, 2019, date of publication July 16, 2019, date of current version August 1, 2019.

Digital Object Identifier 10.1109/ACCESS.2019.2928718

Dynamic Response Analysis for a Terminal Guided Projectile With a Trajectory Correction Fuze

RUPENG LI, DONGGUANG LI, AND JIERU FAN
Science and Technology on Electromechanical Dynamic Control Laboratory, Beijing Institute of Technology, Beijing 100081, China
Corresponding author: Dongguang Li (lidongguang@bit.edu.cn)

ABSTRACT Successful terminal correction without an attitude feedback loop is a challenging task. Much innovative effort is required to achieve a balance between performance and affordability. This paper presents a unique trajectory correction fuze with a reduced number of sensors and actuators. A rapidly calculable analytical dynamic response model for the terminal control force is derived, in which the oscillation part is emphasized because of the limited time-to-go. The accuracy and effectiveness of the analytical model are verified by comparison with 6DOF nonlinear simulations. The influences of the velocity, rotation rate, and pitch on the dynamic response during terminal correction are subsequently investigated using the analytical model. To enable a deep investigation of stability under terminal control with a trajectory correction fuze, the Routh stability criterion is considered to define the necessary prerequisites for stable flight. The validity of the derived instability boundaries is demonstrated through numerical simulations.

INDEX TERMS Dynamic response, terminal guided projectile, trajectory correction fuze, flight stability.

I. INTRODUCTION

A trajectory correction fuze is an effective tool for improving projectile delivery accuracy and reducing collateral damage [1]–[3]. Compared with guided projectiles, trajectory correction fuzes have a unique advantage in that stockpiles can be easily retrofitted and upgraded by simply replacing the trajectory correction fuzes, with no additional modification of the projectile body. Research on ways to ensure that such correction fuzes can meet the requirements of modern warfare in terms of accuracy improvement and reduced expenditure has undergone rapid development in the past twenty years. The main correction strategies used for trajectory correction fuzes can be classified into two types: impact point prediction [4]–[7] and model trajectory tracking [8]–[10]. In impact point prediction, the approximate target coordinates are loaded prior to launch. An onboard ballistic algorithm is used to predict the impact point of the current flight path. The control signal is derived from the deviation between the loaded and predicted impact points. Similarly, in model trajectory tracking, the real-time projectile states are compared with the loaded nominal trajectory states. The difference is used as feedback to correct the trajectory. These two frequently used strategies do not rely on a target detector and thus are inherently limited in terms of accuracy improvement. Consequently, in pursuit of further developments in trajectory correction fuzes, correction schemes based on target imager feedback have begun to be considered. Some recent efforts regarding trajectory correction with imager feedback can be found in references [11] and [12].

The main objects to which trajectory correction fuzes are applied are gun-launched or cannon-launched projectiles, which are always used to strike ground targets. Due to the severe constraints on fuze volume, the field angle and focal length of the target detector are limited, and the corresponding maximal detection range is also limited. Therefore, such correction fuzes are mainly used for terminal guided projectiles. There is no doubt that the successful application of trajectory correction fuzes in terminal guided projectiles has the potential to enable further accuracy improvements. However, it should be noted that conventional projectiles are not provided with a feedback loop for flight attitude. For better correction, the dynamic response must be extensively studied preflight. Many related efforts have been reported in the literature. Mark Costello [13] investigated the influences of control force position and duration on projectile response through numerical calculations. Cooper et al. [14], [15] investigated the effects of different lateral pulse parameters on

The associate editor coordinating the review of this manuscript and approving it for publication was Guiwu Wei.

dynamic response, Ollerenshaw and Costello [8] explained the relationship between the control force and the response direction, and Cooper et al. [16] studied the effects of the center-of-pressure position on the response amplitude and phase. Liu et al. [17] obtained a steady-state analytical solution for the angle of attack under a given control force in the case that gravity and other factors are ignored. Chang [18] considered the coupled effect of the control force and gravity and derived an approximate swerve response expression. Hainz and Costello [19] proposed a modified linear projectile theory to eliminate the accuracy problems in response prediction that arise in the classical linear method when a high elevation is applied. These studies have made significant contributions in this field. However, to the author's knowledge, these efforts have always assumed that the time-to-go for correction is sufficient and have focused only on the steady-state response. In some studies, for simplicity, the oscillation response is ignored entirely. This simplification has always been a good approximation; however, if the subject under investigation were to be a terminal guided projectile with a trajectory correction fuze, the situation would be different. Because of the constraints on the time-to-go in this case, the dynamic response induced by the control force cannot reach the steady state before impact. Thus, the oscillation response in the terminal stage should receive greater attention. The objective of this paper is to bridge this gap and provide supplemental research on the dynamic response of a terminal guided projectile with a trajectory correction fuze.

Additionally, for such a fuze based on imager feedback, the imager must be mounted at the fuze head, and due to the limitations on the volume and monetary cost of fuzes to be used in military operations, the number of other sensors and the complexity of the maneuvering system must be minimized. To this end, in section 2, a novel concept for a trajectory correction fuze based on imager feedback for a terminal guided projectile is proposed, and a general description of its mechanism is presented. The dynamical model of a terminal guided projectile with the proposed fuze is subsequently established. Following sections 1 and 2, the paper proceeds as follows. In section 3, the dynamic response under terminal control exerted by the fuze actuator is derived; here, unique linearized substitutes for the angular rates are introduced to improve the accuracy of the analytical expression. Examples of terminal guided flight simulations are presented to verify the validity and accuracy of the derived analytical model, along with a discussion of the influence of the flight parameters on the dynamic response during correction. In section 4, the stability of the terminal guided projectile is discussed. By converting the stability problem into a mathematical problem, the instability boundaries for the terminal control force are derived based on the Routh stability criterion. In section 5, a conclusion is presented.

II. DYNAMICAL MODEL UNDER CONTROL

This section describes a novel trajectory correction fuze based on detector feedback for the terminal phase. A brief description of its structure follows. The dynamical model of the flight of a projectile under such terminal control is studied and linearized, including the expressions for the aerodynamic forces and moments. The differential equation for the angle of attack is subsequently derived.

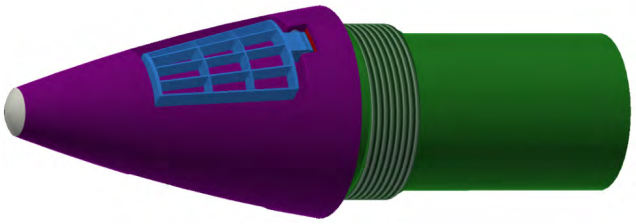

FIGURE 1. Schematic of the trajectory correction fuze with canards attached to the surface.

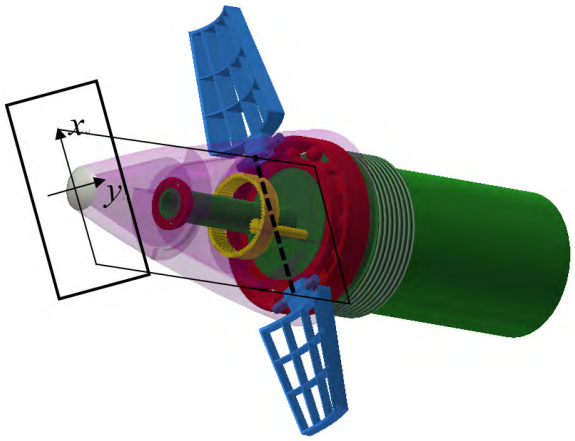

FIGURE 2. Schematic of the trajectory correction fuze with maneuvering components.

A. TRAJECTORY CORRECTION FUZE CONCEPT

The design of the proposed terminal correction fuze is based on imager feedback. A single-axis control actuation system is used to drive the canard rotation. The imager is the sole additional sensor, and it is irrelevant whether the detector signals are laser signals or infrared signals because general seekers can approximately satisfy this design [20]. When the projectile flies without any control, the canards are attached to the fuze surface as shown in Fig. 1. The fuze is divided into two parts. The aft part (green in Fig. 1) is screwed into the projectile body by a threaded connection. The traditional fuze components are contained in the aft part. The forward part can independently rotate relative to the aft part (and the body) by means of a pair of rolling bearings (red in Fig. 2). The outer ring of the bearing is fixed to the internal surface of the forward part of the fuze. The yellow part in Fig. 2 represents the drive shaft of the motor and a pair of internal gears, which are used to drive the rotation of the forward part. Two features of this design should be highlighted: 1. The imager and the canards are both packaged in a strap-down manner in the aft part of the fuze. 2. The line between the installation positions of the two canards (the dashed black

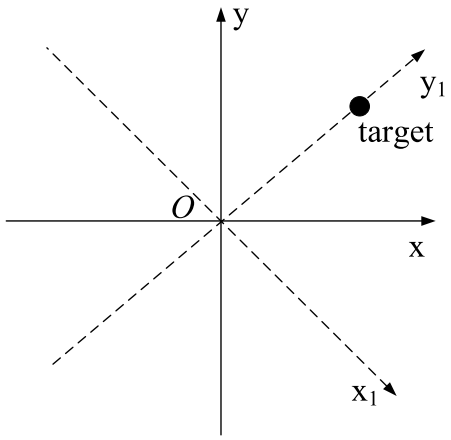

FIGURE 3. The target shown in the detector plane.

line in Fig. 2) is parallel to the horizontal axis of the detector, and both this line and the axis lie in the same horizontal plane, as shown in Fig. 2. The purpose of feature 1 in this design is to ensure that the detector and the canards will rotate with the forward part of the fuze at the same frequency, whereas the purpose of feature 2 is to ensure that the direction of the control force induced by the canards will be perpendicular to the x-axis (e.g., the horizontal axis) of the detector at all times. Once the projectile's flight has reached the terminal phase, the target can be shown in the detector plane x-O-y (as shown in Fig. 3). For correction, the aft part of the fuze rotates until the target falls on the y-axis (e.g., the vertical axis) in the detector plane. Because of the "strapdown" design, the canards rotate through the same angle together with the detector and the fuze. The expected direction of the control force is determined concurrently. To distinguish it from the detector plane before rotation, the detector plane after rotation is represented as x1-O-y1 in Fig. 3. Then, the canards are deployed into the airstream and generate a control force due to the oncoming flow. Because of the unique predetermined installation locations of the canards, the control force can directly correct the terminal trajectory towards the target.

The canards are designed in a waffle style to increase the surface area exposed to the oncoming flow. Considering the limited time-to-go for correction of the terminal trajectory, this design is beneficial because it provides a larger control force compared with the traditional configuration. Each inner grid of the canard has a fixed deflection angle to provide the prerequisites for various strategies. The specific design of the canard parameters is determined by the dynamic response of the projectile. Therefore, an accurate and fast dynamic response expression is critical to the design of the trajectory correction fuze and may be helpful for correction strategies in which real-time calculations are required. From the description of the fuze, it can be seen that the number of sensors is reduced and the complexity of the maneuvering system is minimized. By only utilizing a pair of canards and a single-axis motor, the two dimensional correction can be completed. Moreover, no more actuators are needed to adjust the canard deflection in time during correction because of the fixed deflection design. Thus, this correction fuze can meet volume limit requirements while maintaining a balance between affordability and performance, as is necessary for a terminal guided projectile.

B. FLIGHT MODEL OF THE PROJECTILE UNDER CONTROL

The inertial coordinate is defined firstly: The origin is located at the launch point, x-axis is lied in horizontal plane and points to the target on the ground, z-axis is lied in vertical plane and points down, y-axis is determined by the right-hand rule. The kinematic and dynamic equations of projectile are written in the fixed plane coordinates, which are defined as follows: The origin of the coordinate system is located at the centroid of the projectile. The x-axis is aligned with the longitudinal axis of the projectile, and the positive direction points towards the nose of the projectile. The y-axis is perpendicular to the longitudinal axis and lies in the horizontal plane; the positive direction points to the right. The z-axis is perpendicular to the xy plane, and the positive direction points down. According to the definition, it can be seen the fixed plane coordinate is a non-spinning coordinate.

The equations are divided into two groups: the equations of the center-of-mass motion in Eq. (1)-(2) and the equations of the rotational dynamics in Eq. (3)-(4). Eq (1) and (3) are used to describe projectile dynamics. Eq (2) and (4) are used to describe the kinematics of projectile.

$$\begin{Bmatrix} \dot{u} \\ \dot{v} \\ \dot{w} \end{Bmatrix} = \begin{Bmatrix} F_x/m \\ F_y/m \\ F_z/m \end{Bmatrix} + g \begin{Bmatrix} -\sin\theta \\ 0 \\ \cos\theta \end{Bmatrix} + \begin{Bmatrix} F_{xc}/m \\ F_{yc}/m \\ F_{zc}/m \end{Bmatrix} + \begin{bmatrix} 0 & r & -q \\ -r & 0 & p \\ q & -p & 0 \end{bmatrix} \begin{Bmatrix} u \\ v \\ w \end{Bmatrix} \tag{1}$$

$$\begin{bmatrix} \dot{x} \\ \dot{y} \\ \dot{z} \end{bmatrix} = \begin{bmatrix} \cos\theta\cos\psi & -\sin\psi & \sin\theta\cos\psi \\ \cos\theta\sin\psi & \cos\psi & \sin\theta\sin\psi \\ -\sin\theta & 0 & \cos\theta \end{bmatrix} \begin{bmatrix} u \\ v \\ w \end{bmatrix} \tag{2}$$

$$\begin{Bmatrix} \dot{p} \\ \dot{q} \\ \dot{r} \end{Bmatrix} = \left[I^{-1}\right] \left\{ \begin{Bmatrix} M_x \\ M_y \\ M_z \end{Bmatrix} + \begin{Bmatrix} 0 \\ M_{yc} \\ N_{zc} \end{Bmatrix} - \begin{bmatrix} 0 & -r & q \\ r & 0 & -p \\ -q & p & 0 \end{bmatrix} [I] \begin{Bmatrix} p \\ q \\ r \end{Bmatrix} \right\} \tag{3}$$

$$\begin{bmatrix} \dot{\gamma} \\ \dot{\theta} \\ \dot{\psi} \end{bmatrix} = \begin{bmatrix} 1 & 0 & \tan\theta \\ 0 & 1 & 0 \\ 0 & 0 & 1/\cos\theta \end{bmatrix} \begin{bmatrix} p \\ q \\ r \end{bmatrix} \tag{4}$$

where x, y, z are the components of the projectile position in inertial coordinate. u, v, and w are the components of the projectile velocity in the fixed plane coordinate; p, q, r are the components of the projectile angular velocity in the fixed plane coordinate. In addition, p equals -$r$tanθ. Fx, Fy, and Fz are the components of the aerodynamic forces acting on the projectile body; Mx, My, and Mz are the corresponding moment components. γ, θ, ψ represent roll, pitch and yaw

angle of the projectile respectively. *Fxc Fyc* and *Fzc* are the terminal control force components, which are only exerted during the terminal phase; *Myc* and *Mzc* are the corresponding control moments.

The second and third equations in (1) and (3) represent the dynamic motion in the horizontal and vertical planes. The angle of attack α and the sideslip β are introduced for linearization; they are defined in (5) and (6).

$$\alpha = \arctan^{-1}\left(\frac{w}{V}\right) \approx \frac{w}{V} \tag{5}$$

$$\beta = \arctan^{-1}\left(\frac{v}{V}\right) \approx \frac{v}{V} \tag{6}$$

$$\begin{cases} \dot{\beta} = \dfrac{F_y}{mv} + \dfrac{F_{yc}}{mv} - r \\ \dot{\alpha} = \dfrac{F_z}{mv} + \dfrac{F_{zc}}{mv} + \dfrac{g}{v}\cos\theta + q \\ \dot{q} = \dfrac{M_y + M_{yc}}{I_Y} - pr\dfrac{I_{xx}}{I_{yy}} \\ \dot{r} = \dfrac{M_z + M_{zc}}{I_Y} + pq\dfrac{I_{xx}}{I_{yy}} \end{cases} \tag{7}$$

Then, the four equations can be rewritten in terms of α and β. $r\tan\theta$ and its related terms can be regarded as small quantities and ignored, thus yielding the set of linearized equations shown in (7).

The aerodynamic forces in (7) include the drag force, the lift force and the Magnus force (always treated as a small quantity and ignored), while the aerodynamic moments include the static moment, pitch damping moment, damping moment and Magnus moment, for which the corresponding expressions are shown below:

$$\begin{cases} F_y = -\dfrac{1}{2}\rho SV^2 C_{l\alpha}\beta - \dfrac{1}{2}\rho SV^2 C_D\beta - \dfrac{1}{2}\rho SV^2 C_{yp\alpha}\dfrac{pl}{V}\alpha \\ F_z = -\dfrac{1}{2}\rho SV^2 C_{l\alpha}\alpha - \dfrac{1}{2}\rho SV^2 C_D\alpha + \dfrac{1}{2}\rho SV^2 C_{yp\alpha}\dfrac{pl}{V}\alpha \\ M = \dfrac{1}{2}\rho SlV^2 C_{M\alpha}\alpha + \dfrac{1}{2}\rho SlV^2 C_{Mp\alpha}\dfrac{pl}{V}\beta + \dfrac{1}{2}\rho SlV^2 C_{Mq}\dfrac{l}{V}q \\ N = -\dfrac{1}{2}\rho SlV^2 C_{M\alpha}\beta + \dfrac{1}{2}\rho SlV^2 C_{Mp\alpha}\dfrac{pl}{V}\alpha + \dfrac{1}{2}\rho SlV^2 C_{Mq}\dfrac{l}{V}r \end{cases} \tag{8}$$

ρ is the air density, S is the reference area of the projectile, d is the projectile diameter, V is the projectile velocity, l is the reference length of the projectile, and the notations involving C represent the aerodynamic parameters of the projectile.

As mentioned in section 2.1, the designed canard has a fixed deflection angle. Once it is unfolded, the control force and moment can be generated. The expression of induced control force and control moment are shown in

$$\begin{aligned} F_{yc} &= \frac{1}{2}\rho V^2 S_C\left(2C_{N\delta}\right)\delta_C \sin\gamma_C \\ F_{zc} &= \frac{1}{2}\rho V^2 S_C\left(2C_{N\delta}\right)\delta_C \cos\gamma_C \end{aligned} \tag{9}$$

$$\begin{aligned} M_{yc} &= x_C\frac{1}{2}\rho V^2 S_C\left(2C_{N\delta}\right)\delta_C \cos\gamma_C \\ M_{zc} &= x_C\frac{1}{2}\rho V^2 S_C\left(2C_{N\delta}\right)\delta_C \sin\gamma_C \end{aligned} \tag{10}$$

In which $C_{N\delta}$ means the normal force coefficient for a single canard, δ_C means the deflection angle of the canard, S_C means the reference area of the canard, x_C means the distance from the canard location to the centroid.γ_C means the roll angle of the canard. It is determined by the detection information of the target orientation. It should be noted that, the parameters ρ, S_C are constant. δ_C is also invariable because of the design of fixed deflection angle. For terminal guided projectile, the time-to-go is limited, so the coefficient $C_{N\delta}$ can be regarded as a constant within this duration. For the same reason, we take the same approach of Frank Fresconi [11] and regard parameter V as a constant, which equals the initial velocity during the correction. So for a short time-to-go, the control force and control moment for correction are assumed as invariable for convenience. For the projectile with low speed, the time-to-go may be not sufficiently short. In such a situation, the relative parameter should be updated according to the specific requirements.

It should be noted that the design of the novel fuze with reduced complexity is applicable for terminal guided projectiles. However, the design makes the canard deflection unchangeable, and the control force cannot be adjusted in time during the correction. So common correction strategies are not suitable any more. For this design, the roll angle of the canard and the unfolding time are used as inputs of control system. The former is used to determine the control force direction, and the latter is used to determine the correction duration according to various needed miss distance. More details of the new correction strategy can be found in reference [21]. In this paper, we pay more attention on the dynamic response for the projectile under terminal control with limited time-to-go.

The response equation for the complex angle of attack under control can be obtained from the four equations in (7). The second and third equations are multiplied by the complex operator i, and the results are added to the first and fourth equations. By ignoring the products and high-order exponentials of small quantities, the differential equation for the complex angle of attack is obtained.

$$\begin{aligned} &\ddot{\Delta} + \left(k_{zz} + b_y - iP\right)V\dot{\Delta} - \left(M + iPT\right)V^2\Delta \\ &= -\ddot{\theta} - \dot{\theta}\left(k_{zz} - iP\right)V + \frac{\left(M_{yc} + iM_{zc}\right)}{I_{yy}} + \frac{i(F_{yc} + iF_{zc})I_{xx}p}{mI_{yy}V} \end{aligned} \tag{11}$$

For a more simplified expression, the time infinitesimal is substituted by an arc, as shown in (12).

$$\begin{aligned} \frac{d\Delta}{dt} &= \frac{d\Delta}{ds}\frac{ds}{dt} = V\Delta' \\ \frac{d^2\Delta}{dt} &= \frac{d\left(V\Delta'\right)}{ds}\cdot\frac{ds}{dt} \end{aligned} \tag{12}$$

The velocity equation is necessary and supplemented here.

$$V' = -b_x V - \frac{g\sin\theta}{V} \tag{13}$$

With Eq (12)-(13), the coefficients of the independent variable in Eq (11) are substituted by constants in a short interval. The resulting linear equation is (14).

$$\Delta'' + (H - iP)\,\Delta' - (M + iPT)\Delta = C \tag{14}$$

The related parameters are shown below.

$$\begin{aligned} H &= b_y + k_{zz} - b_x - \frac{2g\sin\theta}{V^2}, \\ M &= k_z,\ T = b_y - \frac{I_{yy}}{I_{xx}}k_y,\ P = \frac{I_{xx}p}{I_{yy}V} \\ C &= -\frac{\ddot{\theta}}{V^2} - \frac{\dot{\theta}}{V}(k_{zz} - iP) + \frac{(M_{yc} + iM_{zc})}{I_{yy}V^2} \\ &\quad + \frac{i(F_{yc} + iF_{zc})I_{xx}p}{mI_{yy}V^3} \end{aligned} \tag{15}$$

where $b_x = \frac{\rho S}{2m}C_D$ $b_y = \frac{\rho S}{2m}C'_y$ $k_z = \frac{\rho Sl}{2I_{yy}}m'_z$ $k_{zz} = \frac{\rho Sld}{2I_{yy}}m'_{zz}$ $k_y = \frac{\rho Sld}{2I_{yy}}m'_y$,$m$ is the projectile mass, I_{yy} is the moment of inertia around the transverse axis of the projectile, and I_{xx} is the moment of inertia around the longitudinal axis of the projectile.

III. ANALYTICAL DYNAMIC RESPONSE AND VERIFICATION

In this section, an analytical expression is derived for the dynamic response of a terminal guided projectile. In previous research in this field, a sufficient time-to-go has always been assumed when obtaining such response expressions; however, this assumption is not applicable for terminal correction. To address this issue, this assumption is relinquished when deriving the effective analytical expression in this section. Furthermore, periodic updating of the trajectory parameters, as is commonly done, is no longer necessary because of the proposed linear substitute for the angular rate.

A. RESPONSE EXPRESSION FOR TERMINAL CORRECTION

When the parameters in (14) are treated as constant over a short interval, the solution to this ordinary differential equation is obtained as shown in (16).

$$\Delta = C_1 e^{l_1 s} + C_2 e^{l_2 s} + \Delta_p \tag{16}$$

Here, l_1 and l_2 are expressed in terms of the parameters H, P, M, and T as shown below:

$$l_{1,2} = \frac{1}{2}(-H + iP \pm \sqrt{4M + H^2 - P^2 + 2iP(2T - H)}) \tag{17}$$

By extracting the real and imaginary parts of l1 and l2, we can define λ and ω as shown in (18). From a mathematical perspective, λ represents the damping of the complex angle of attack, while ω represents the angular rate. Specifically, λ_1 and ω_1 represent the fast epicyclic motion, and λ_2 and ω_2 represent the slow epicyclic motion.

$$\begin{aligned} l_1 &= \lambda_1 + \omega_1 i \\ l_2 &= \lambda_2 + \omega_2 i \end{aligned} \tag{18}$$

The solution for the complex angle of attack consists of two parts. The first and second terms on the right-hand side of (16) are induced by the initial disturbance and represent the oscillating part of the response, which decays with time. Therefore, this part of the solution has always previously been neglected to facilitate the analysis. However, for a terminal guided projectile, the oscillation cannot be ignored because of the limited time available for correction. The third term is induced by the control force and gravity and represents the steady-state part of the response. Δ_P is derived and expressed directly as shown in (19).

$$\begin{aligned} \Delta_P = &\frac{\left[\ddot{\theta} + V\dot{\theta}\,(k_{zz} - iP)\right]}{V^2(M^2 + P^2T^2)} \\ &- \frac{\left[mV(M_{yc} + iM_{zc}) + iI_{yy}p(F_{yc} + iF_{zc})\right](M - iPT)}{mI_{YY}V^3(M^2 + P^2T^2)} \end{aligned} \tag{19}$$

Because it is reasonable to assume that the launching and meteorological conditions are ideal, the initial angle-of-attack response and its derivatives can be assumed to be zero. Accordingly, C_1 and C_2 are as shown in (20).

$$\begin{aligned} C_1 &= C_{1r} + C_{1i}i = -\frac{l_2\Delta_p}{l_2 - l_1} \\ C_2 &= C_{2r} + C_{2i}i = -\frac{l_1\Delta_p}{l_1 - l_2} \end{aligned} \tag{20}$$

It is obvious that C_1 and C_2 are influenced by the steady-state conditions. The subscripts i and r indicate the values of the imaginary and real parts, respectively. Through the calculation above, the components of the complex angle of attack in the horizontal and vertical planes are decoupled in this paper.

$$\begin{aligned} \alpha = &e^{\lambda_1 t}(C_{1r}\cos\omega_1 t - C_{1i}\sin\omega_1 t) \\ &+ e^{\lambda_2 t}(C_{2r}\cos\omega_2 t - C_{2i}\sin\omega_2 t) + \Delta_{P\alpha} \end{aligned} \tag{21}$$

$$\begin{aligned} \beta = &e^{\lambda_1 t}(C_{1r}\cos\omega_1 t + C_{1i}\sin\omega_1 t) \\ &+ e^{\lambda_2 t}(C_{2r}\cos\omega_2 t + C_{2i}\sin\omega_2 t) + \Delta_{P\beta} \end{aligned} \tag{22}$$

The steady-state components of the angle of attack and sideslip in expressions (21) and (22) can be derived from (19) as shown in (23) and (24).

$$\begin{aligned} \Delta_{P\alpha} = &\frac{\ddot{\theta} + V\dot{\theta}k_{zz}}{V^2\left(M^2 + P^2T^2\right)} \\ &- \frac{\left(mVM_{yc} - I_{xx}pF_{zc}\right)M + \left(mVM_{zc} + I_{xx}pF_{yc}\right)PT}{mI_{yy}V^3\left(M^2 + P^2T^2\right)} \end{aligned} \tag{23}$$

$$\begin{aligned} \Delta_{P\beta} = &\frac{-VP\dot{\theta}}{V^2\left(M^2 + P^2T^2\right)} \\ &- \frac{\left(mVM_{zc} + I_{xx}pF_{yc}\right)M - \left(mVM_{yc} - I_{xx}pF_{zc}\right)PT}{mI_{yy}V^3\left(M^2 + P^2T^2\right)} \end{aligned} \tag{24}$$

The trajectory shift response is derived subsequently in this section. Because the aerodynamic forces and moments exerted on the projectile (e.g., the lift force, drag force, and Magnus force) are directly correlated with the angle of attack and sideslip, the expression for the trajectory shift response of the terminal guided projectile can be derived as shown in (25). The horizontal and vertical components are given by (26) and (27).

$$S_C = \sqrt{y^2 + z^2} \tag{25}$$

$$y = \iint (\frac{1}{2}\rho S(C_{l\alpha}\beta + C_D\beta + C_{yp\alpha}\frac{pl}{V}\alpha) + \frac{F_{yc}}{mV^2})ds \tag{26}$$

$$z = \iint (\frac{1}{2}\rho S(C_{l\alpha}\alpha + C_D\alpha + C_{yp\alpha}\frac{pl}{V}\beta) + \frac{F_{zc}}{mV^2} - \frac{g\cos\theta}{V^2})ds \tag{27}$$

From the response expressions (14) and (15), it is evident that the oscillation part of the response is closely related to the angular rates ω. For a clearer investigation of the oscillation part, the angular rates ω are expanded as shown in (28), where $A = 1 - \frac{4M}{P^2} - \frac{H^2}{P^2}$ $B = \frac{-4T+2H}{P}$. By ignoring small-quantity terms and expanding the expression under the root into a series, the ω expressions can be simplified.

$$\omega_1 = \frac{P}{2}\left[1 + \sqrt{\frac{A + \sqrt{A^2 + B^2}}{2}}\right] \approx P$$
$$\omega_2 = \frac{P}{2}\left[1 - \sqrt{\frac{A + \sqrt{A^2 + B^2}}{2}}\right] \approx \frac{M}{P} \tag{28}$$

It should be noted that the angular rates vary with time. In general, the influence of ω on the response is ignored because the oscillation response decays with time. However, for a terminal guided projectile, neglecting this variation may gradually result in inaccuracy of the approximate analytical solution. To derive a more practical analytical solution for a terminal guided projectile, the error induced by the angular rate variation should be minimized. Updating the trajectory parameters periodically along the trajectory may be a solution to this problem. However, the repeated stopping and restarting during the calculation process that such periodic updates would necessitate would inevitably complicate the analytical method. When real-time calculations are required, this approach would increase the onboard computational costs. Therefore, this paper proposes a rapid computing method for terminal guided projectiles. Because the increase in M in (28) over a short time interval can be ignored for a terminal guided projectile, ω_1 and ω_2 are monotonic and can be considered to have high linearity. For simplicity, the variations in ω_1 and ω_2 with time are substituted by linear functions, of which the intercepts b and the slopes k are derived via linear fits. The substituted linear functions are written as $\omega_1 = k_{\omega_1}t + b_{\omega_1}$ and $\omega_2 = k_{\omega_2}t + b_{\omega_2}$, and are used as time-dependent self-compensation terms for the angular rates. The validity and feasibility of this simplified linear substitution will be verified later. The newly derived expressions for the angle of attack and sideslip are given in (29) and (30).

$$\alpha = e^{\lambda_1 t}(C_{1r}\cos(k_{\omega_1}t + b_{\omega_1})\,t - C_{1i}\sin(k_{\omega_1}t + b_{\omega_1})t) + e^{\lambda_2 t}(C_{2r}\cos(k_{\omega_2}t + b_{\omega_2})t - C_{2i}\sin(k_{\omega_2}t + b_{\omega_2})t) + \Delta_{P\alpha} \tag{29}$$

$$\beta = e^{\lambda_1 t}(C_{1r}\cos(k_{\omega_1}t + b_{\omega_1})t + C_{1i}\sin(k_{\omega_1}t + b_{\omega_1})t) + e^{\lambda_2 t}(C_{2r}\cos(k_{\omega_2}t + b_{\omega_2})t + C_{2i}\sin(k_{\omega_2}t + b_{\omega_2})t) + \Delta_{P\beta} \tag{30}$$

It should be noted that the assumption of sufficient time to reach the steady state is relinquished and the oscillation part of the response is highlighted in these terminal response expressions. Therefore, the analytical response model presented in this paper is applicable to terminal guided projectiles.

TABLE 1. Projectile physical parameters.

Initial conditions		Meteorological conditions	
Velocity	250 m/s	Ground pressure	1000 hPa
Pitch	-43°	Virtual temperature	288.9
Direction	0°	Longitudinal wind	0 m/s
Spin-rate	1050 rad/s	Lateral wind	0 m/s

B. EXAMPLE SIMULATIONS AND VERIFICATION

The feasibility and accuracy of the simplified analytical model derived in section 3 are verified in this section. A simulation of nonlinear 6DOF rigid equations is treated as the ground-truth model for validating the method. The simulation solver used is a fourth-order Runge-Kutta solver, and the step size is 0.001 s. Some relevant parameters of the example terminal guided projectile are given as follows: the mass is 15 kg, the moment of inertia around the longitudinal axis is 0.023 kg·m^2, the moment of inertia around the transverse axis is 0.22 kg·m^2, the reference area is 0.087 m^2, the projectile diameter is 0.0105 m, and the time-to-go for correction is 6 s. The initial and meteorological condition parameters are listed in table 1.

To better demonstrate the validity and effectiveness of the analytical response model, angular motion results with no external control force are first presented in Fig. 4 and Fig. 5, where the solid red lines represents the sideslip and angle-of-attack responses computed via the numerical 6DOF simulation. It is clear that the oscillation cannot be neglected.

Before verifying the analytical model, we verify the validity of the linear substitution for the angular rates presented in section 3.1. A comparison for the example trajectory demonstrates the practical applicability of this substitution method. The results are shown in Fig. 7, where the solid red lines represent the solutions for ω over time from (28) for the terminal guided projectile and the dashed blue lines represent the linear functions obtained by fitting the discrete solution points. It is obvious that the difference between the two lines

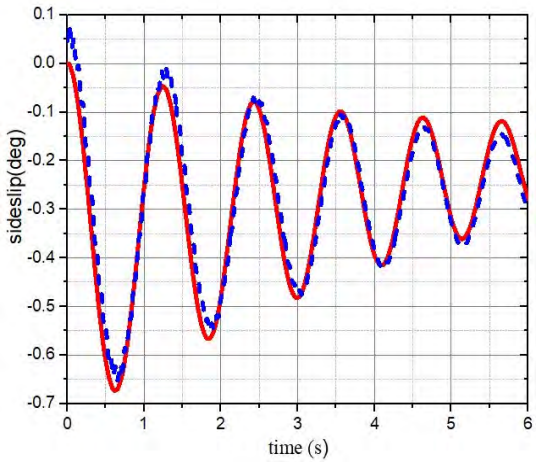

FIGURE 4. Sideslip versus time for a ballistic trajectory.

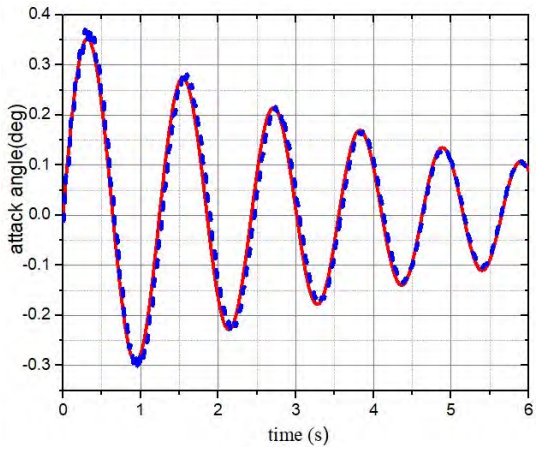

FIGURE 5. Angle of attack versus time for a ballistic trajectory.

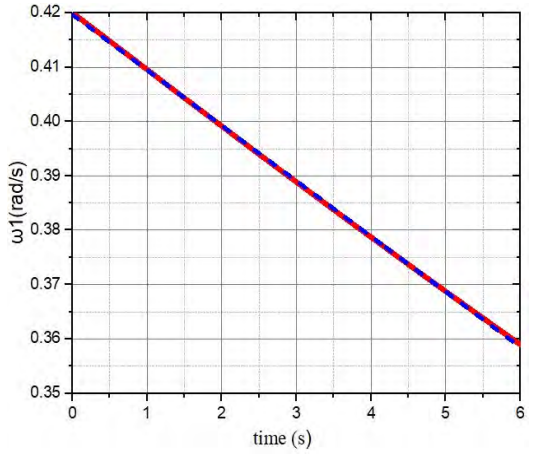

FIGURE 6. ω_1 versus time for a terminal guided projectile.

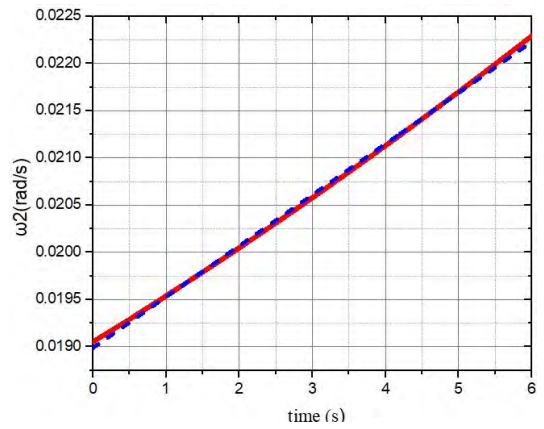

FIGURE 7. ω_2 versus time for a terminal guided projectile.

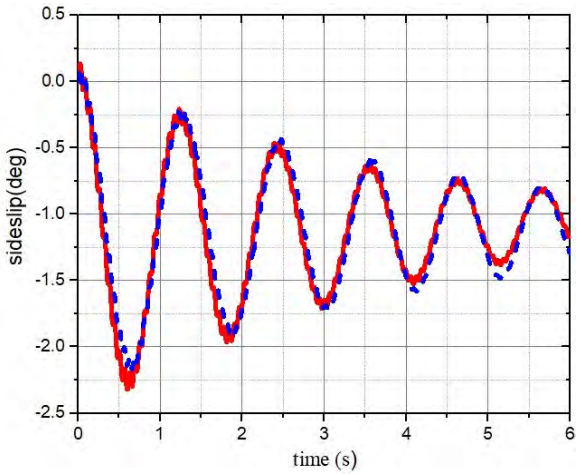

FIGURE 8. Sideslip response versus time under a 10 N control force.

is very small, indicating that the simplified linear substitution is applicable in the following study.

Now, let us verify the analytical model with angular rate substitute. The dashed blue lines in Fig. 6 and Fig. 7 represent the results computed with the modified model. As shown, the analytical results agree well with the sideslip and angle-of-attack responses derived from the 6DOF model.

For further investigation, a similar comparison for the angular motion response under a 10 N rightward horizontal control force is illustrated in Fig. 8 and Fig. 9, and a comparison for a 20 N leftward horizontal control force is illustrated in Fig. 10 and Fig. 11. The meanings of the lines in these two figures are the same as those in Fig. 4 and Fig. 5; to avoid repetition, they are not described again. As shown, the analytical solutions and the true values exhibit good agreement over time. Thus, the effectiveness of the analytical response model for angular motion prediction is verified for both ballistic and controlled trajectories.

Now, let us compare the analytical trajectory shifts derived in this paper with the numerical 6DOF nonlinear results. In Fig. 12, no additional control force is acting on the projectile during the terminal phase, while in Fig. 13 and Fig. 14, horizontal 10 N and −20 N control forces are exerted, respectively. The solid red lines represent the true values computed from the 6DOF rigid ballistic equations, and the dashed blue lines represent the results computed from the

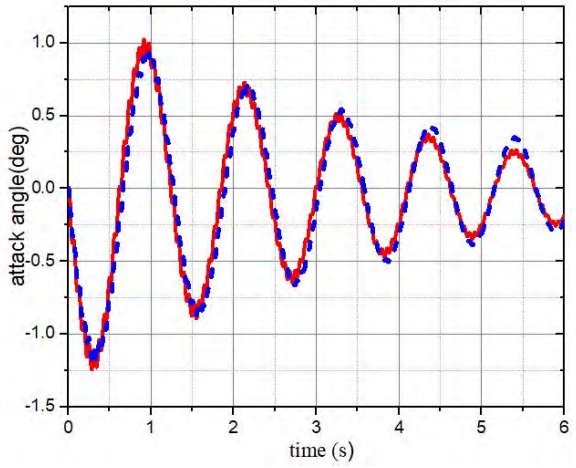

FIGURE 9. Angle-of-attack response versus time under a 10 N control force.

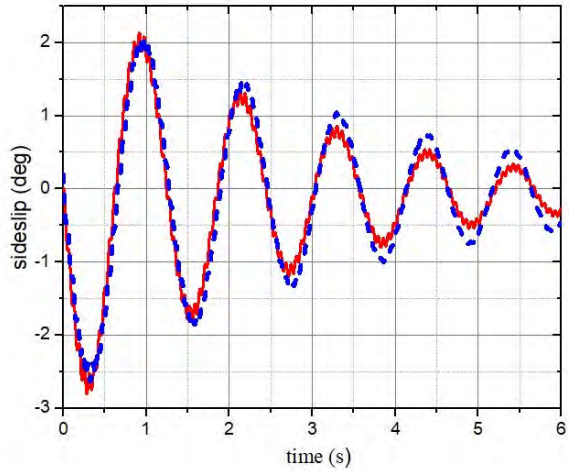

FIGURE 10. Sideslip response versus time under a −20 N control force.

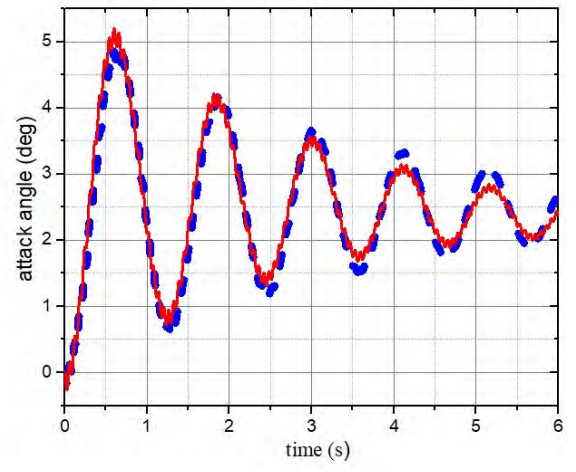

FIGURE 11. Angle-of-attack response versus time under a −20 N control force.

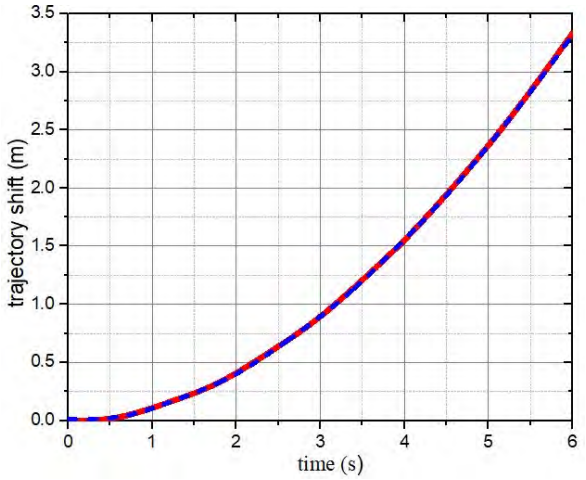

FIGURE 12. Trajectory shift versus time for a ballistic trajectory.

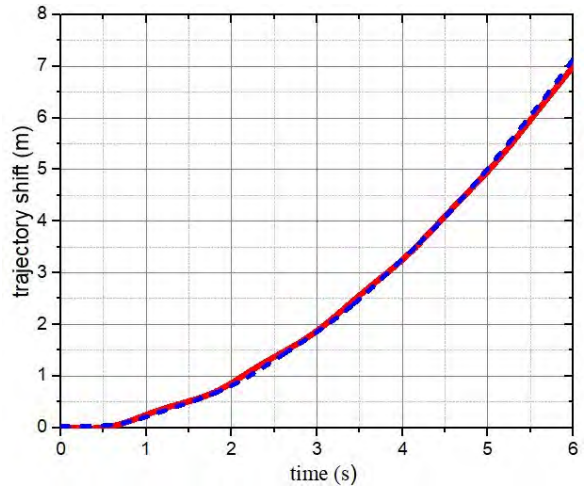

FIGURE 13. Trajectory shift versus time under a 10 N control force.

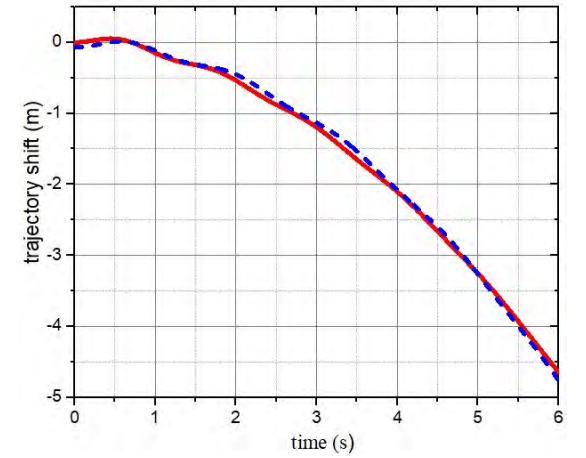

FIGURE 14. Trajectory shift versus time under a −20 N control force.

analytical response model. As illustrated, the simplified analytical model is able to accurately predict the trajectory shift for a terminal guided projectile.

Overall, the accuracy and effectiveness of the analytical model are demonstrated by these simulation results, and it is concluded that the proposed analytical model can satisfy the

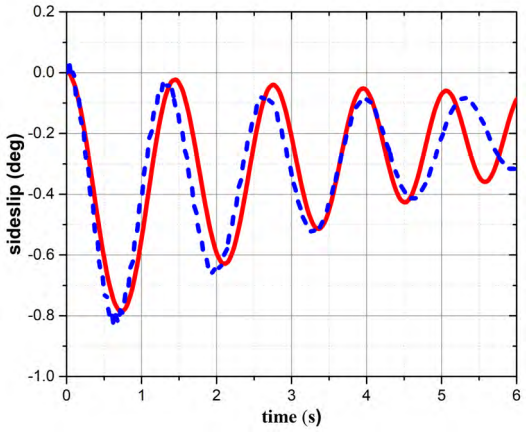

FIGURE 15. Sideslip versus time for a ballistic trajectory.

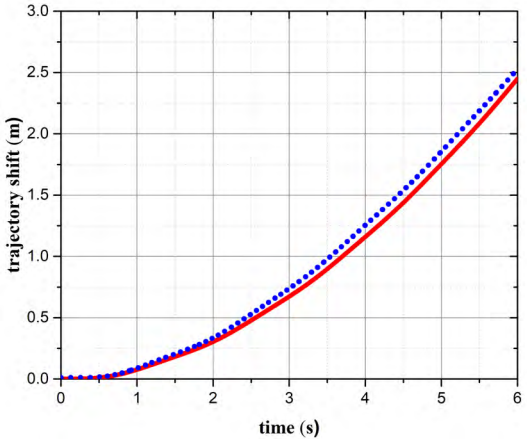

FIGURE 17. Trajectory shift versus time for a ballistic trajectory.

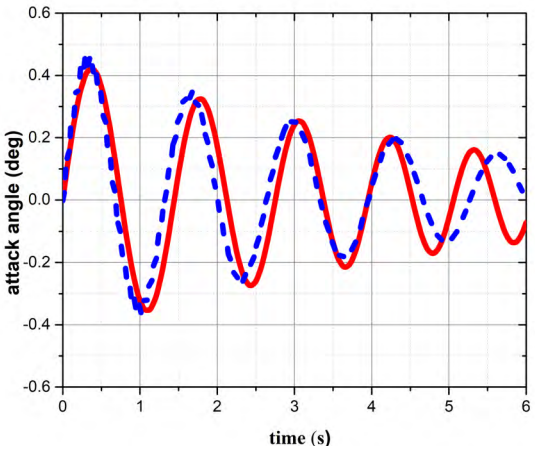

FIGURE 16. Angle of attack versus time for a ballistic trajectory.

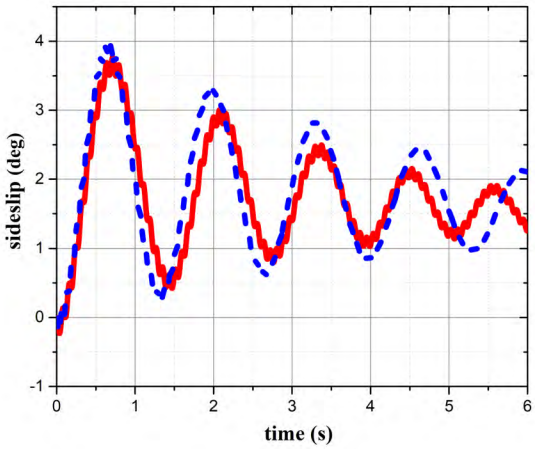

FIGURE 18. Sideslip response versus time under a 10 N control force.

requirements of response analysis for terminal guided projectiles. Moreover, it is useful for real-time correction strategies and the aerodynamic design of the control actuators.

It should be noticed that although the analytical solution is well verified by the simulations, we find that the analytical angular motion prediction in Fig 9 and Fig 10 is gradually deviating from the true value from the fifth second. For a more comprehensive verification, another set of simulations under different initial conditions are implemented. In these simulations, the projectile velocity is 200m/s, the pitch angle is -55 degree, the spin-rate is 800rad/s.

Fig. 15 and Fig. 16 illustrate the angular motions under the new initial conditions. The red line represents the result derived from numerical 6DOF model. Blue line represents the analytical result. In the first four seconds, although the deviation from true value is bigger when compared with the last set of simulations, the analytical solution can still predict the angular motion with a relatively small error. However, in the last 1.5 second, the deviation becomes evident. The trajectory shift is shown in Fig. 17. The maximum error between the analytical result and true value is about 8.4%. the final calculation error of the results between the analytical model and nonlinear 6DOF rigid model is 3.2%.

When a 10N control force is exerted as a control force, the angular motions under new initial conditions are shown in Fig. 18 and Fig. 19. It can be seen the results of the controlled trajectory are similar with that of a ballistic trajectory. The analytical solutions almost agree with that from a numerical 6DOF model. But the track deviates gradually after about 4.5 seconds. Fig. 20 represents the comparison of the trajectory shift under control. The maximum error is about 9.3%. the final calculation error of the results between the analytical model and nonlinear 6DOF rigid model is 6.1%.

From the simulations and verifications we find that the oscillation response is a indispensable part in terminal guidance. the proposed method is used to predict the response in an analytical way. It should be mentioned that the analytical method proposed in this paper is based on linearization. So the parameters of the differential equation can be regarded as constant. The simulation results shows that it is well used in a short interval. It can be seen, however, in some specific cases, the calculation accuracy may be decreased as time goes by. The reason is that the valid intervals for calculation are

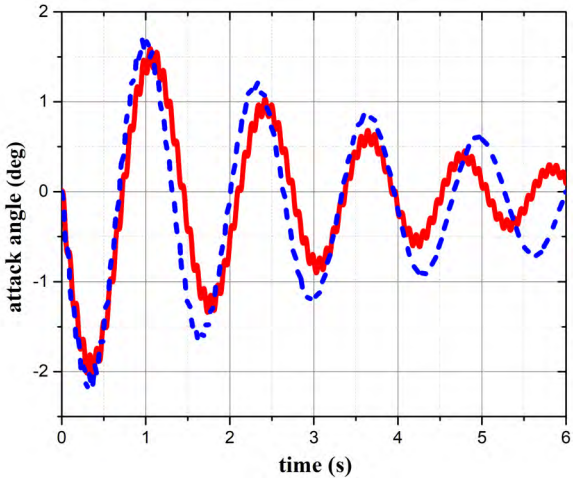

FIGURE 19. Angle-of-attack response versus time under a 10 N control force.

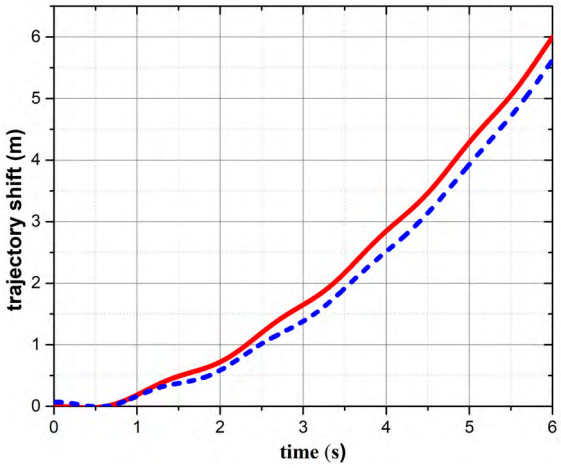

FIGURE 20. Trajectory shift versus time under a 10 N control force.

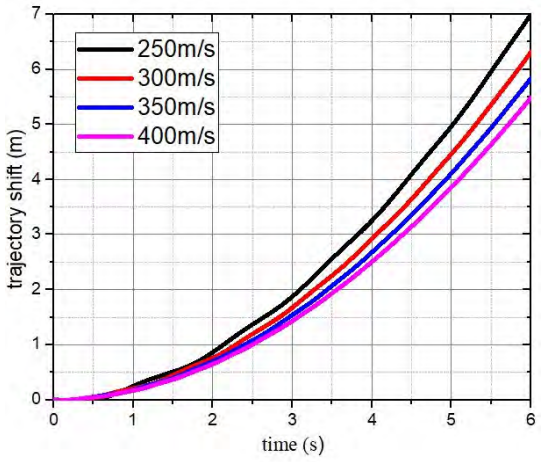

FIGURE 21. Shift response with velocity during correction.

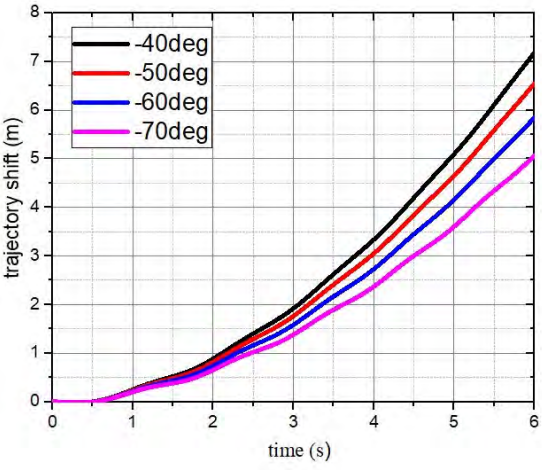

FIGURE 22. Shift response with pitch angle during correction.

different according to the variation of the physical properties and initial conditions of projectiles. Fortunately, the correction time for terminal guidance is limited. So it is applicable in such a situation. For the projectile with low terminal velocity, the flight time is longer, and one parameter update for the analytical expression may be necessary.

C. ANALYSIS AND DISCUSSION

By analyzing the dynamic response model derived in this paper, it is found that the control force is not the only factor influencing the dynamic response. Other parameters, such as the initial velocity and the rotation rate and pitch during terminal correction, also influence the response. Here, we present a detailed study of the dynamic response of the trajectory shifts for a terminal guided projectile with different parameters using the analytical model.

We take the projectile considered in section 3.2 as an example. A constant 10 N control force in the horizontal plane begins to be exerted on the projectile with only 6 s left. We consider several values of the projectile velocity at the initiation of control: 250 m/s, 300 m/s, 350 m/s and 400 m/s. Fig. 21 shows the variation in the trajectory shift response with these different terminal velocities. For the same control force, the trajectory shift response for the controlled projectile increases as the terminal velocity decreases. From the perspective of the analytical model, the reason for this behavior is that the quadratic and cubic velocity terms are negatively correlated with the trajectory response. Now, let us consider the influence of the pitch angle on the response. For a terminal guided projectile, correction always begins in the descending stage. Therefore, we consider the following values of the initial pitch angle during the terminal phase: $-40°$, $-50°$, $-60°$, and $-70°$. Fig. 22 shows that the shift increases as the pitch angle decreases. Similarly, to investigate the influence of the rotation rate on the trajectory shift for a terminal guided projectile, the analytical solutions for controlled projectiles under different rotation rates are compared. As shown in Fig. 23, a higher rotation rate results in a larger shift response.

These comparisons based on the analysis of the dynamic response model illustrate that when investigating the dynamic response under control, all of the parameters mentioned above should be considered. These results are also

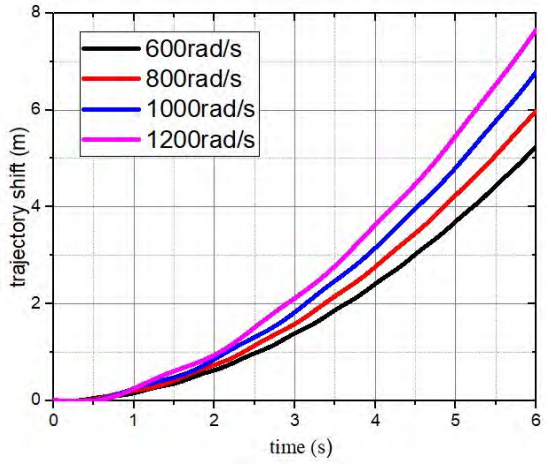

FIGURE 23. Shift response with rotation rate during correction.

helpful for research on correction strategies for terminal guided projectiles.

IV. STABILITY ANALYSIS

The relationship between the dynamic response and the control force was investigated in section 3. This relationship can play a significant role in research on terminal correction. However, flight stability is a prerequisite for successful correction. There is no doubt that the control force can also influence the flight stability. For a standard precision-guided weapon, an attitude loop, a sophisticated actuator and various sensors can be used together to maintain a balance between maneuverability and stability for the controlled projectile. Therefore, the influence of the force magnitude on the flight stability is not a critical issue and is always ignored because the flight time is sufficient and the flight attitude can be adjusted in real time. Consequently, the control frequency and the attitude angle have received the most attention in previous stability research [22], [23]. However, for a terminal guided projectile with the trajectory correction fuze proposed in section 2, a simple control strategy without an attitude loop is always used; thus, the influence of the force magnitude must be considered preflight. In this section, this issue is investigated by deriving the instability boundaries for the control force magnitude.

Generally, divergent angular motion over time indicates unstable flight. Because expression (7) in section 2 is used to describe the angular motion, it is recalled in this section and rewritten in matrix form as follows:

$$\dot{X} = KX + Q$$

The full expression is shown in (31).

$$\begin{bmatrix} \dot{\beta} \\ \dot{\alpha} \\ \dot{q} \\ \dot{r} \end{bmatrix} = \begin{bmatrix} k_1 & k_2 & 0 & -1 \\ -k_2 & k_1 & 1 & 0 \\ k_4 & k_3 & k_5 & 0 \\ -k_3 & k_4 & 0 & k_5 \end{bmatrix} \begin{bmatrix} \beta \\ \alpha \\ q \\ r \end{bmatrix} + \begin{bmatrix} \dfrac{F_{yc}}{mV} \\ mg\cos\theta + \dfrac{F_{zc}}{mV} \\ \dfrac{M_C}{I_Y} \\ \dfrac{N_C}{I_X} \end{bmatrix} \tag{31}$$

where

$$k_1 = -\frac{\rho SVC_{l\alpha}}{2m} - \frac{\rho SVC_D}{2m} k_2 = -\frac{\rho SC_{yp\alpha} pl}{2m} k_3 = \frac{\rho SlV^2 C_{M\alpha}}{2I_Y}$$
$$k_4 = \frac{\rho Sl^2 VC_{MP\alpha} p}{2I_Y} k_5 = \frac{\rho Sl^2 VC_{Mq}}{2I_Y}$$

K is the state matrix of the angular motion of the projectile, and the subscripted k parameters represent the state coefficients. By deriving the characteristic equation for K, we can convert the stability problem into a mathematical problem that can be solved by analyzing the state matrix. However, it is evident that the control force does not appear in the matrix K. This implies that the control force has no effect on flight stability, which is contrary to reality. The main cause of this phenomenon is investigated below.

The fixed plane coordinate system has a roll rate $r\tan\theta$ relative to the inertial coordinate system. This roll rate is required to keep the y-axis of the fixed plane located in the horizontal plane. The linearized expression given in (31) is derived by ignoring $r\tan\theta$ and its related terms, which is always an effective approach in angular motion research. However, as illustrated above, this linearization causes difficulty in stability analyses because the assumption violates the requirement and forces the fixed plane coordinate system to rotate at a rate of $r\tan\theta$. As a result, the directions of the control force and gravity vary with the fixed plane coordinates, and this variation should be reflected in the linearized equation. Therefore, we propose an angular compensation matrix. We define the roll angle Φ induced by the linearization, the expression for which is given in (32), and use it to write the compensation matrix given in (33). This compensation matrix should be applied before linearization.

$$\dot{\Phi} = r\tan\theta \tag{32}$$

$$T_m = \begin{bmatrix} 1 & 0 & 0 \\ 0 & \cos\Phi & \sin\Phi \\ 0 & -\sin\Phi & \cos\Phi \end{bmatrix} \tag{33}$$

With this compensation matrix, the translational motion of the projectile can be rewritten as shown in Eq. (34).

$$\begin{Bmatrix} \dot{u} \\ \dot{v} \\ \dot{w} \end{Bmatrix} = \begin{Bmatrix} F_x/m \\ F_y/m \\ F_z/m \end{Bmatrix} + g \begin{bmatrix} 1 & 0 & 0 \\ 0 & \cos\Phi & \sin\Phi \\ 0 & -\sin\Phi & \cos\Phi \end{bmatrix} \begin{bmatrix} -\sin\theta \\ 0 \\ \cos\theta \end{bmatrix} + \begin{bmatrix} 1 & 0 & 0 \\ 0 & \cos\Phi & \sin\Phi \\ 0 & -\sin\Phi & \cos\Phi \end{bmatrix} \begin{bmatrix} F_{xc}/m \\ F_{yc}/m \\ F_{zc}/m \end{bmatrix} + \begin{Bmatrix} 0 & r & -q \\ -r & 0 & -r\tan\theta \\ q & r\tan\theta & 0 \end{Bmatrix} \begin{Bmatrix} u \\ v \\ w \end{Bmatrix} \tag{34}$$

Similarly, the angular motion of the projectile can be rewritten as shown in Eq. (35).

$$\begin{Bmatrix} \dot{p} \\ \dot{q} \\ \dot{r} \end{Bmatrix} = \left[I^{-1}\right] \left\{ \begin{Bmatrix} L \\ M \\ N \end{Bmatrix} + \begin{bmatrix} 1 & 0 & 0 \\ 0 & \cos\Phi & \sin\Phi \\ 0 & -\sin\Phi & \cos\Phi \end{bmatrix} \begin{bmatrix} L_c \\ M_c \\ N_c \end{bmatrix} - \begin{bmatrix} 0 & -r & q \\ r & 0 & r\tan\theta \\ -q & -r\tan\theta & 0 \end{bmatrix} [I] \begin{Bmatrix} p \\ q \\ r \end{Bmatrix} \right\} \tag{35}$$

Then, linearization is performed. The projectile velocity V and roll rate p are treated as constant over a sufficiently short time interval. Suppose that the velocity component u is equal to V. The pitch angle θ can be substituted by $\theta_0 + \theta_d$, where θ_0 is the initial pitch angle and θ_d is the departure from θ_0, which is small. It should be noted that this method is applicable only within a few seconds of the selected feature point. Fortunately, the time-to-go for terminal correction is limited to several seconds, so this method is reasonable. The linear ballistic differential equations are eventually derived as shown in Eq. (36)-(39).

$$\dot{\beta} = \frac{F_y}{mV} + (\frac{F_{zc}}{mV} + \frac{g}{V}\cos\theta_0)\Phi - r + \frac{F_{yc}}{mV} \tag{36}$$

$$\dot{\alpha} = \frac{F_z}{mV} + \frac{F_{zc}}{mV} + \frac{g}{V}\cos\theta_0 + q - \frac{F_{yc}}{mV}\Phi - (\frac{g}{V}\sin\theta_0)\theta_d \tag{37}$$

$$\dot{q} = \frac{M}{I_Y} - pr\frac{I_X}{I_Y} + \frac{M_c}{I_Y} + \frac{N_c}{I_Y}\Phi \tag{38}$$

$$\dot{r} = \frac{N}{I_Y} + pq\frac{I_X}{I_Y} + \frac{N_c}{I_Y} - \frac{M_c}{I_Y}\Phi \tag{39}$$

By combining the four equations above with Eq. (32) and the supplemental Eq. (40), the set of equations is completed.

$$\dot{\theta}_d = q \tag{40}$$

Rewriting the set of equations Eq. (32)-Eq. (40) in the matrix form

$$\dot{K} = KX + Q \tag{41}$$

yields the following:

$$\begin{bmatrix} \dot{\beta} \\ \dot{\alpha} \\ \dot{q} \\ \dot{r} \\ \dot{\Phi} \\ \dot{\theta}_d \end{bmatrix} = \begin{bmatrix} k_1 & k_2 & 0 & -1 & k_6 & 0 \\ k_2 & k_1 & 1 & 0 & k_7 & k_8 \\ k_4 & k_3 & k_5 & -k_{11} & k_9 & 0 \\ -k_3 & k_4 & k_{11} & k_5 & k_{10} & 0 \\ 0 & 0 & 0 & \tan\theta_0 & 0 & 0 \\ 0 & 0 & 1 & 0 & 0 & 0 \end{bmatrix} \begin{bmatrix} \beta \\ \alpha \\ q \\ r \\ \Phi \\ \theta_d \end{bmatrix} + \begin{bmatrix} \frac{F_{yc}}{mV} \\ \frac{F_{zc}}{mV} + \frac{g}{V}\cos\theta_0 \\ \frac{M_C}{I_Y} \\ \frac{N_C}{I_X} \\ 0 \\ 0 \end{bmatrix} \tag{42}$$

where the new notations are defined as follows:

$$k_6 = \frac{F_{ZC}}{mV} + \frac{g}{V}\cos\theta_0 \; k_7 = -\frac{F_{YC}}{mV} \; k_8 = -\frac{g}{V}\sin\theta_0 \; k_9 = \frac{N_C}{I_Y} \; k_{10} = -\frac{M_C}{I_Y} \; k_{11} = p\frac{I_X}{I_Y}$$

It can be seen that terms related to the control force now appear in the state coefficient matrix K because of the compensation matrix, and thus, the problem is transformed into an algebraic stability problem. Characteristic polynomial for the coefficient matrix in Eq. (42) is established as follows:

$$\det(\lambda E - A) = a_6\lambda^6 + a_5\lambda^5 + a_4\lambda^4 + a_3\lambda^3 + a_2\lambda^2 + a_1\lambda + a_0 \tag{43}$$

where a_0-a_6 represent the state coefficients. By ignoring secondary factors, the expressions for a_0-a_6 after simplification can be written as follows:

$$\begin{cases} a_6 = 1 \\ a_5 = -2k_1 - 2k_5 \\ a_4 = k_{11}^2 - 2k_3 - k_{10}\tan\theta_0 \\ a_3 = -2k_1k_{11}^2 + 2k_1k_3 + 2k_3k_5 + 2k_4k_{11} - k_9k_{11}\tan\theta_0 \\ a_2 = k_3^2 + k_3k_{10}\tan\theta_0 - k_4k_9\tan\theta_0 + 2k_1k_9k_{11}\tan\theta_0 \\ a_1 = k_3^2k_8 - k_3^2k_6\tan\theta_0 - k_1k_3k_{10}\tan\theta_0 + k_3k_8k_{10}\tan\theta_0 \\ a_0 = -k_1k_3k_8k_{10}\tan\theta_0 - k_3^2k_6k_8\tan\theta_0 \end{cases} \tag{44}$$

The Routh matrix corresponding to the characteristic equation is given in Eq. (45).

$$T_{ROUTH} = \begin{bmatrix} a_6 & a_4 & a_2 & a_0 \\ a_5 & a_3 & a_1 & \\ b_1 = \frac{-1}{a_5}(a_6a_3 - a_5a_4) & b_2 = \frac{-1}{a_5}(a_6a_1 - a_2a_5) & b_3 = a_0 & \\ c_1 = \frac{-1}{b_1}(a_5b_2 - a_3b_1) & c_2 = \frac{-1}{b_1}(a_5b_3 - a_1b_1) & & \\ d_1 = \frac{-1}{c_1}(b_1c_2 - b_2c_1) & d_2 = a_0 & & \\ e_1 = \frac{-1}{d_1}(c_1d_2 - c_2d_1) & & & \\ f_1 = a_0 & & & \end{bmatrix} \tag{45}$$

The necessary prerequisites for stable controlled flight are given by the Routh stability criterion: the coefficients a_0-a_6 in Eq. (43) must be positive, and the elements in the first column of the Routh matrix must be positive. In other words, if the control force magnitude does not satisfy Eq. (46), then the projectile will lose stability. In this case, the control force is characterized as an unstable force. The set of all unstable forces is called the unstable scope. The boundaries of this scope are called the instability boundaries. If a control force magnitude lies within the unstable scope, it can be directly concluded that the flight is definitely unstable.

$$\begin{cases} a_5 > 0, a_4 > 0, a_3 > 0, a_2 > 0, a_1 > 0, a_0 > 0 \\ b_1 > 0, c_1 > 0, d_1 > 0, e_1 > 0 \end{cases} \tag{46}$$

The example projectile considered in section 3 is used here to verify the instability boundaries. According to the research of Lloyd and Brown [24], projectiles under control are most sensitive to horizontal forces. Therefore, the simulations in this section focus on the effect of the horizontal control force *Fyc*. The unstable scope computed for *Fyc* is $[-\infty, -35.48] \cup [58.33, +\infty]$. If the control force magnitude

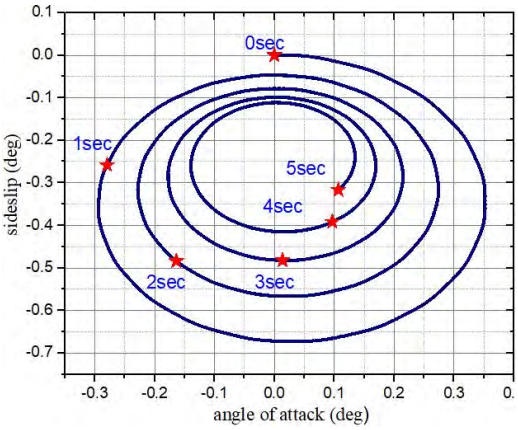

FIGURE 24. Angular motion for a flight without a control force.

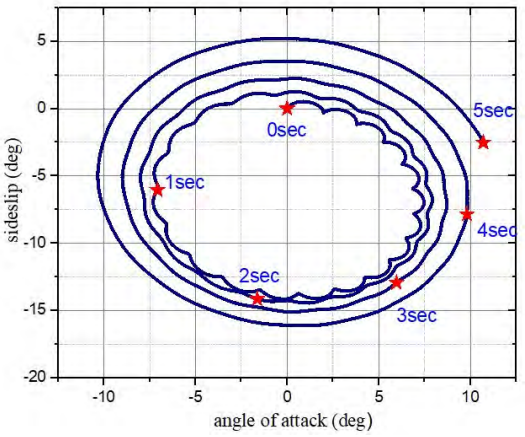

FIGURE 25. Angular motion for a flight with a −40 N control force.

derived in accordance with the theory presented in section 3 lies within this unstable scope, then the projectile will lose stability.

First, as a basis for comparison, the angular motion of the projectile without a control force is presented in Fig. 24. This figure illustrates that the angular motion during a flight without a control force converges gradually over time, corresponding to stable flight. The angular motion of the same projectile under a −40 N leftward force during terminal correction is presented in Fig. 25. The results illustrate that the fast epicyclic motion of the projectile is stable. However, the slow epicyclic motion markedly diverges over time, i.e., is unstable. Finally, the results of applying a 60 N terminal control force in the simulation are shown in V; these results indicate that the slow epicyclic motion of the projectile is stable, while the fast epicyclic motion is unstable. Because stable flight implies the simultaneous stability of both the slow and fast epicyclic motions, both situations correspond to unstable flight. Thus, the validity of the proposed instability boundaries is demonstrated for the values of −40 and 60 N, which lie in the positive and negative parts of the unstable scope, respectively.

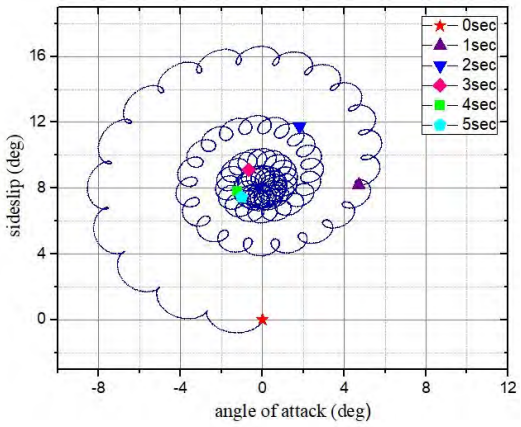

FIGURE 26. Angular motion for a flight with a 60 N control force.

V. CONCLUSION

A novel trajectory correction fuze with an imager sensor is proposed for a terminal guided projectile. The strapdown design of the detector and the waffle canards is useful for achieving two-dimensional trajectory correction with limited volume requirements and at a low cost. The dynamic response to the terminal control force is studied. Because of the limited time-to-go for correction, the oscillation response is emphasized. A linear substitution for the angular rate variation is introduced in the analytical expressions to improve the accuracy of the response prediction. Moreover, the real-time periodic updating of the trajectory parameters is no longer necessary in the derived analytical model. The analytical solution is compared with the 6DOF nonlinear solution. The results show that the analytical solution agrees well with the simulation result. Based on the analytical model of the dynamic response, the influences of the velocity, pitch and rotation rate are discussed. To make the research more comprehensive, the Routh stability criterion is considered to define the necessary prerequisites for stable flight under control, and the instability boundaries for the control force are derived. This research is expected to be helpful in guiding the design of canard parameters and correction strategies for terminal guided projectiles with trajectory correction fuzes.

APPENDIX

$C_{l\alpha}$	= Lift force coefficient
C_D	= Drag force coefficient
$C_{yp\alpha}$	= Magnus force coefficient derivative
$C_{M\alpha}$	= Static moment coefficient derivative
$C_{Mp\alpha}$	= Magnus moment coefficient derivative
C_{Mq}	= Damping moment coefficient derivative induced by the pitch and yaw rates
u, v, w	= Components of the projectile velocity along the x-, y-, and z-axes in the fixed plane coordinates, m/s
F_x, F_y, F_z	= Components of the aerodynamic forces on the projectile body along the x-, y-, and z-axes in the fixed plane coordinates, N

F_{yc}, F_{zc} = Components of the control forces on the projectile body along the y- and z-axes in the fixed plane coordinates, N
p, q, r = Components of projectile angular rate in the fixed plane coordinates, rad/s
M_x, M_y, M_z = Components of the aerodynamic moments acting on the projectile body along the x-, y-, z-axes in the fixed plane coordinates, Nm
M_{yc}, M_{zc} = Components of the control moments acting on the projectile body along the y- and z-axes in the fixed plane coordinates, Nm
V = Projectile velocity, m/s
θ = Projectile pitch angle, rad
g = Gravitational acceleration, m/s^2
ρ = Atmospheric density, kg/m^3
S = Projectile reference area, m^2
l = Projectile reference length, m
I_{xx} = Moment of inertia around the longitudinal axis of the projectile, kg·m^2
I_{yy} = Moment of inertia around the transverse axis of the projectile, kg·m^2
$[I]$ = Diagonal inertia matrix
ω_1 = Angular rate of slow epicyclic motion
ω_2 = Angular rate of fast epicyclic motion

REFERENCES

[1] G. Eric and M. Lauzon, "Course correction fuze concept analysis for in-service 155 mm spin-stabilized gunnery projectiles," in *Proc. AIAA Guid. Navigat. Control Conf. Exhib.*, Aug. 2008, p. 6997. doi: 10.2514/6.2008-6997.

[2] Y. Wang, W.-D. Song, D. Fang, and Q.-W. Guo, "Guidance and control design for a class of spin-stabilized projectiles with a two-dimensional trajectory correction fuze," *Int. J. Aerosp. Eng.*, vol. 2015, Jul. 2015, Art. no. 908304.

[3] S. Theodoulis, F. Sève, and P. Wernert, "Robust gain-scheduled autopilot design for spin-stabilized projectiles with a course-correction fuze," *Aerosp. Sci. Technol.*, vol. 42, pp. 477–489, Apr./May 2015.

[4] F. Fresconi, "Guidance and control of a projectile with reduced sensor and actuator requirements," *J. Guid., Control, Dyn.*, vol. 34, no. 6, pp. 1757–1766, 2011. doi: 10.2514/1.53584.

[5] F. Fresconi and P. Plostins, "Control mechanism strategies for spin-stabilized projectiles," *Proc. Inst. Mech. Eng. G, J. Aerosp. Eng.*, vol. 224, no. 9, pp. 979–991, 2010. doi: 10.1243/09544100JAERO705.

[6] K. B. Pamadi and E. Ohlmeyer, "Evaluation of two guidance laws for controlling the impact flight path angle of a naval gun launched spinning projectile," in *Proc. AIAA Guid. Navigat. Control Conf. Exhib.*, Aug. 2006, p. 6081. doi: 10.2514/6.2006-6081.

[7] C. Phillips, "Guidance algorithm for range maximization and time-of-flight control of a guided projectile," *J. Guid., Control, Dyn.*, vol. 31, no. 5, pp. 1447–1455, 2008. doi: 10.2514/1.31327.

[8] D. Ollerenshaw and M. Costello, "Model predictive control of a direct fire projectile equipped with canards," *J. Dyn. Syst. Meas. Control*, vol. 130, no. 6, 2008, Art. no. 061010. doi: 10.1115/1.2957624.

[9] T. Jitpraphai and M. Costello, "Dispersion reduction of a direct fire rocket using lateral pulse jets," *J. Spacecraft Rockets*, vol. 38, no. 6, pp. 929–936, 2001. doi: 10.2514/2.3765.

[10] J. Rogers and M. Costello, "Design of a roll-stabilized mortar projectile with reciprocating canards," *J. Guid., Control, Dyn.*, vol. 33, no. 4, pp. 1026–1034, 2010. doi: 10.2514/1.47820.

[11] F. Fresconi and J. Rogers, "Flight control of a small-diameter spin-stabilized projectile using imager feedback," *J. Guid., Control, Dyn.*, vol. 38, no. 2, pp. 181–191, 2015. doi: 10.2514/1.G000815.

[12] F. Fresconi, C. Gene, I. Celmins, J. De Spirito, and M. Costello, "Flight mechanics of a novel guided spin-stabilized projectile concept," in *Proc. AIAA Atmos. Flight Mech. Conf.*, Aug. 2010, p. 7639. doi: 10.2514/6.2010-7638.

[13] M. Costello and A. Peterson, "Linear theory of a dual-spin projectile in atmospheric flight," *J. Guid., Control, Dyn.*, vol. 23, no. 5, pp. 789–797, 2000. doi: 10.2514/2.4639.

[14] G. R. Cooper and M. Costello, "Flight dynamic response of spinning projectiles to lateral impulsive loads," *J. Dyn. Syst. Meas. Control*, vol. 126, no. 3, pp. 605–613, 2004.

[15] B. J. Guidos and G. R. Cooper, "Linearized motion of a fin-stabilized projectile subjected to a lateral impulse," *J. Spacecraft Rockets*, vol. 39, no. 3, pp. 384–391, 2015. doi: 10.2514/2.3837.

[16] G. Cooper, F. Fresconi, and M. Costello, "Flight stability of an asymmetric projectile with activating canards," *J. Spacecraft Rockets*, vol. 49, no. 1, pp. 130–135, 2015. doi: 10.2514/1.A32022.

[17] X.-D. Liu, D.-G. Li, and Q. Shen, "Swerving orientation of spin-stabilized projectile for fixed-cant canard control input," *Math. Problems Eng.*, vol. 2015, Mar. 2015, Art. no. 173571. doi: 10.1155/2015/173571.

[18] S. Chang, "Dynamic response to canard control and gravity for a dual-spin projectile," *J. Spacecraft Rockets*, vol. 53, no. 3, pp. 558–566, 2016. doi: 10.2514/1.A33485.

[19] L. Hainz and M. Costello, "Modified projectile linear theory for rapid trajectory prediction," *J. Guid., Control, Dyn.*, vol. 28, no. 5, pp. 1006–1014, 2005. doi: 10.2514/1.8027.

[20] M. Goldshtein, Y. Oshman, and T. Efrati, "Seeker gyro calibration via model-based fusion of visual and inertial data," in *Proc. AIAA Guid. Navigat. Control Conf. Exhib.*, Aug. 2008, p. 7424.

[21] R. Li, D. Li, and J. Fan, "Correction strategy of mortars with trajectory correction fuze based on image sensor," *Sensors*, vol. 19, no. 5, p. 1211, 2019. doi: 10.3390/s19051211.

[22] P. Wernert, "Stability analysis for canard guided dual-spin stabilized projectiles," in *Proc. AIAA Atmos. Flight Mech. Conf.*, 2009, p. 5843. doi: 10.2514/6.2009-5843.

[23] D. Zhu, S. Tang, and J. Guo, "Flight stability of a dual-spin projectile with canards," *Proc. Inst. Mech. Eng. G, J. Aerosp. Eng.*, vol. 229, no. 4, pp. 704–716, 2015. doi: 10.1177/0954410014539293.

[24] K. H. Lloyd and D. P. Brown, "Instability of spinning projectiles during terminal guidance," *J. Guid. Control*, vol. 2, no. 1, pp. 65–70, 1979. doi: 10.2514/3.55833.

RUPENG LI was born in 1991. He received the master's degree in mechatronical engineering from the Tianjin University of Technology, in 2015. He is currently pursuing the Ph.D. degree in navigation guidance and control with the Beijing Institute of Technology. He has published some papers in international journals and conferences.

DONGGUANG LI was born in 1965. He is currently a Professor with the Department of Mechatronical Engineering, Beijing Institute of Technology, Beijing, China. He has published 50 papers in international journals.

JIERU FAN was born in 1989. She received the master's degree in applied mathematics from the North University of China, in 2015. She is currently pursuing the Ph.D. degree in unmanned systems with the Beijing Institute of Technology. She has published some papers in international journals and conferences.